The Astronomical Journal, 157:240 (10pp), 2019 June https://doi.org/10.3847/1538-3881/ab1b0f
© 2019. The American Astronomical Society. All rights reserved.

A Decade of Sporadic Meteoroid Mass Distribution Indices in the Southern Hemisphere Derived from SAAMER's Meteor Observations

D. Janches[1], C. Brunini[2,3], and J. L. Hormaechea[3,4]
[1] ITM Physics Laboratory, Heliophyscs Science Division, GSFC/NASA, Greenbelt, MD 20771, USA; diego.janches@nasa.gov
[2] AGGO, CONICET, Villa Elisa, Pcia. de Buenos Aires, Argentina; claudiobrunini@yahoo.com
[3] Facultad de Ciencias Astronómicas y Geofísicas, Universidad Nacional de La Plata, Argentina
[4] Estacion Astronomica Rio Grande, Rio Grande, Tierra del Fuego, Argentina; jlhormaechea@gmail.com
Received 2019 March 14; revised 2019 April 16; accepted 2019 April 17; published 2019 May 23

Abstract

We present determinations of the meteoroid differential mass index, s, using over a decade of meteor observations from the Southern Argentina Agile MEteor Radar (SAAMER). For this, we employ an autonomous statistical technique to determine this parameter from the measured radar echo amplitudes. Unlike previous studies, we examine the role of the system noise in the determination of this parameter and found that if not taken into account appropriately, the results can yield significant over estimations of the mass index. In general we found that a value of $s = 2.0$ represents SAAMER's results in general agreement with recent studies performed in the northern hemisphere. We explore both the index interannual and seasonal variability and, unlike previous studies, we found them to be constant, except during the presence of the Southern δ Aquariids meteor shower which is so strong that it dominates the meteor counts when present. Our study suggests that using the maximum echo amplitude for these studies is not ideal as it can be biased by many factors which make the inaccuracies larger than the precision estimated by the fitting routine. A method that results in a more direct estimate of the electron line density would be required which takes into account range, gain pattern, system noise, etc.

Key words: meteorites, meteors, meteoroids – methods: data analysis – methods: observational – techniques: radar astronomy – zodiacal dust

1. Introduction

Meteoroids from the Sporadic Meteor Complex (SMC) originate from the collision of asteroids and the disintegration of comets. The orbital characteristics of these meteoroids have evolved significantly from the moment of ejection and thus, a direct link to their original progenitor body is generally very difficult to establish. Nevertheless, these particles evolve in such a way that they can be categorized, in a general manner, in relation to the type of bodies they originated from. Specifically, from the point of view of ground-based radar and optical observations, the SMC is observed as six main directional enhancements of the meteor radiants (i.e., orbital families) known as: the north and south Apex, composed mainly of dust from long-period comets (Sekanina 1976; Nesvorný et al. 2011b); the Helion and Antihelion, composed of dust from short-period comets (Hawkins 1956; Weiss & Smith 1960; Nesvorný et al. 2010, 2011a); and the north and south Toroidal, which have been recently associated with dust from Halley-type comets (Pokorný et al. 2014).

Recently, several efforts have been made in modeling these sources using dynamical models of dust evolution from different cometary families and constrain them with both spaceborne and ground-based observations (Nesvorný et al. 2010, 2011a, 2011b; Pokorný et al. 2014). One critical characteristic of the SMC, or any other meteoroid population (e.g., showers), which is essential to these models, is the size or mass-frequency distribution (S/MFD) of meteoroids, which is commonly assumed to be a power law distribution. Previous modeling work of the SMC such as those reported by Nesvorný et al. (2010, 2011a), have assumed this distribution to be a broken law composed of two single power distributions, where the meteoroid size at the breaking point have been argued to be between 30 and 100 μm in diameter, according to different measurement constrains (Ade et al. 2014; Janches et al. 2015b, 2017). However, results from ground-based observations (Blaauw et al. 2011b; Pokorný & Brown 2016) such as those presented here, have suggested that a single power law is a good approximation for submillimeter particles and thus more recent models have adopted this simpler approach (Janches et al. 2018; Pokorný et al. 2018). Under such assumption, the MFD can be described as

$$dN \propto M^{-s} dM, \tag{1}$$

where dN is the number of particles with masses between M and $M + dM$, and s is the differential mass index. The mass index is an essential characteristic of the meteoroid environment because it describes the balance between different sizes within a certain population of particles. For example, if s is equal to 2, it represents a population where the masses are equally distributed per decade of mass. Smaller values of s represent populations in which larger particles are dominant, typical of younger meteor showers and streams (Blaauw et al. 2011a) where enough time has not yet passed to produce smaller particles from collisions. Regarding the SMC, different studies in the past decades have yield values ranging from 2 to 2.34 (see Blaauw et al. 2011b for a summary of these works) suggesting a much older environment dominated by smaller particles.

For the purpose of this work, it is important to distinguish between the original S/MFD describing the particles at the moment of release from the source (Fulle et al. 1995, 2016; Rotundi et al. 2015) and that measured at a particular location of the solar system (i.e., at 1 au; Love & Brownlee 1993; Galligan & Baggaley 2004; Blaauw et al. 2011b; Pokorný &

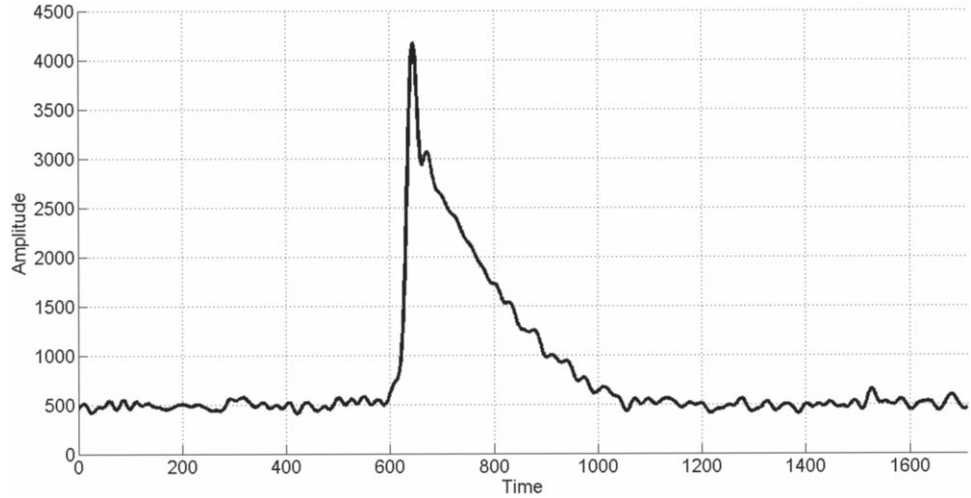

Figure 1. Example of an underdense meteor echo power profile.

Brown 2016, among others). For a review of these measurements and their differences, the reader may refer to Pokorný et al. (2018). For the near-Earth meteoroid environment, ground-based measurements of this parameter are commonly performed with radars and optical techniques, with the most recent studies using the Canadian Meteor Orbit Radar (CMOR) by Blaauw et al. (2011a, 2011b) and Pokorný & Brown (2016). The latter presented 5 yr of radar data allowing the study of both intra- and interannual variability of this parameter. They also presented a brief study of s using optical observations with the Canadian Automated Meteor Observatory (CAMO; Weryk et al. 2013). Using optical observations allowed the authors to extend the mass range for which this variable was determined. These studies were performed in the northern hemisphere. In the southern hemisphere, the most recent studies of s were performed using the Advanced Meteor Orbit Radar (AMOR; Baggaley et al. 1994) reported by Baggaley (1999) and Galligan & Baggaley (2004). This particular study was performed with only a half million of detections and did not provide any interannual information.

Performing these studies at both hemispheres is critical because the presence of different showers and streams can potentially yield differences in the results. In addition, some of the sources are either better observed (i.e., north and south Apex) or not observed at all (i.e., north and south Toroidal) depending on the location of the radar (Campbell-Brown & Wiegert 2009; Janches et al. 2015a). Multi-year observations are also critical due to the sometimes highly variable activity of showers and streams, which again can bias the results. It has also been argued that solar activity affecting the upper atmosphere density profile will affect the altitude at which meteors ablate (e.g., where they are detected), potentially affecting the determination of the mass index (Pokorný & Brown 2016).

In this paper we present an entire solar cycle worth of observations ($\sim$11 yr) using the Southern Argentina Agile MEteor Radar (SAAMER). As in Pokorný & Brown (2016), we developed a reproducible and autonomous statistical technique to determine s from the measured radar maximum echo amplitudes. Like in previous studies, we account for biases in the determination of s introduced by the presence of meteor showers and detected range. However, unlike past studies, we examine the role on the system noise in the determination of this parameter and found that if not taken into account appropriately, the results can also yield significant over estimations. We described the SAAMER system in Section 2 and our statistical methodology in Section 3. The results are presented in Section 4. Discussion of the results as well as comparison with previous studies are presented in Section 5. Finally, Section 6 provides the concluding remarks.

2. SAAMER System Overview

SAAMER has been performing meteor observations since 2008 May in Rio Grande (53° 45′ 8″S; 67° 45′ 5″W), province of Tierra del Fuego, Argentina, at the Estacion Astronómica Rio Grande. SAAMER's original design is enhanced, relative to standard meteor radars, because its initial goal was to measure gravity wave (GW) momentum fluxes in the mesosphere and lower thermosphere atmospheric region (Fritts et al. 2010a, 2010b). These measurements require (1) significantly higher meteor counts (i.e., by at least an order of magnitude) and (2) a need for the majority of meteor detections to be at small zenith (high elevation) angles. These requirements were achieved by having a greatly enhanced transmitter peak power (60 kW, rather than 6–20 kW used by most meteor radar systems) together with the use of a transmitter antenna array composed of eight (instead of one) three-element crossed yagis arranged in a circle of diameter 27.6 m. SAAMER's operating frequency and bandwidth are 32.55 and 0.3 MHz, respectively. SAAMER transmits a 2-km-long pulse with opposite phasing of every other yagi, directing the majority of radar power into eight beams at 45° azimuth increments, with peak power at 35° off zenith. This results in a majority of meteor detections at off-zenith angles between 15° and 50°. However, the system is sufficiently agile such that the phases between the transmitting antennas can be changed to transmit different radiation patterns (Janches et al. 2014). The receiving array is formed by the typical five-antenna interferometer arrangement (Hocking et al. 1997; Jones et al. 1998), all of which are also three-element crossed yagis, enabling redundant meteor position definition with errors less than 0°.5. The data utilized in this work were obtained utilizing the basic echo detection and analysis algorithms for the SKiYMET systems developed by Hocking et al. (2001), which selects echoes that present underdense power return profiles and are optimal for

mesospheric wind measurements (Figure 1). Specifically to this work, these algorithms determine, for the selected echoes, the time of occurrence and location of the echo (i.e., range and azimuth and elevation angles). From these the altitude can also be determined as well as the returned signal amplitude and the signal-to-noise ratio (S/N). In addition, the software flags the level of ambiguity for which the echo position was determined. For this study we only utilized echoes for which their position was determined unambiguously.

For the five-antenna interferometry, unambiguous solutions can be guaranteed only if there are no phase errors. If there are errors (and phase errors in measurements up to 30° and more are quite normal; W. Hocking 2019, personal communication) then ambiguities must arise. The SKYiMET software Skiycorr recognizes this, which is necessary for a proper analysis. Once phase errors are considered, a given meteor can have one of two possible angular positions which cannot be resolved. Furthermore, there is also the possibility of range errors—meteors low to the horizon can have two possible ambiguous heights when the radar transmits at high pulse repetition frequency (PRF), as it is the case for SAAMER's first decade of operation. For example a meteor at a range of 370 km could also quite satisfactorily have been at a range of 441 km if the PRF is 2143 Hz—both would give heights in the range 70–110 km, which cannot be untangled. This could introduce further biases to the determination of s since, as it will be described, it requires a particular selection of ranges.

Currently the system has, in addition, three remote receiving stations, two deployed in 2010 August and a third one in 2017 January, which are utilized to detect the meteor forward scatter signals from meteor trails. The information provided by the outlying receiving stations enables the determination of the time differences between the detection at different sites and from that the meteoroid trajectory and absolute speeds can be derived, which ultimately provide the determination of their orbital parameters (Baggaley et al. 1994; Webster et al. 2004; Janches et al. 2015a). SAAMER has recorded over 7 million orbits since 2012 January. However, for the purpose of this work we only utilized the echoes detected by the main station.

3. Methodology

For the case of underdense meteor echoes detected from the radar specular backscattered signal, it has been argued that the measured signal amplitude is proportional to the electron line density, q, averaged over the first Fresnel zone along the trail (McKinley 1961). In principle, utilizing models, this quantity can be related to the meteoroid mass. However, in this work we focus, as previously done by, for example, Baggaley (1999), Blaauw et al. (2011a, 2011b), and Pokorný & Brown (2016), on determining the differential mass distribution index of the detected meteors rather than the mass of individual meteoroids using the cumulative distribution of the received maximum echo amplitude as a proxy for the mass distribution. The method, which has been described by several authors (Jones 1968; McIntosh & Simek 1969; Blaauw et al. 2011b; Weryk et al. 2013; Pokorný & Brown 2016), assumes that

$$N \propto A^{-(s-1)}, \tag{2}$$

where A is the peak radar maximum amplitude of the detected echo and N is the cumulative number of echoes with peak amplitude greater than A. Equations (1) and (2) assume that the mass distribution of detected meteoroids is described by a single power law and thus there is no change in s across the dynamic range of masses encompassed by the equivalent amplitude range of the radar (Pokorný & Brown 2016). Hence, by recording the amplitude distribution from a shower or for the sporadic background, the slope of a plot of $\log N$ versus $\log A$ will simply be $1 - s$. It is important to note that Equation (2) is applicable only to underdense echoes for which the electron density is low enough that scattering occurs throughout the width of the trail, and thus the amplitude is proportional to q, which in turn is assumed to be proportional to the mass. More detailed discussions regarding Equations (1) and (2) can be found in, for example, Blaauw et al. (2011b) and Pokorný & Brown (2016). Here we just simple adopt the same principles discussed in those works.

Figure 2 displays measurements gathered by SAMMER with solar longitudes (λ_0) between 50° and 51° in 2008 on a log–log scale. The straight line in panel (a) of this figure represents the least-squares linear fit of all the samples in the panel. The deviations of the samples from this straight line, i.e., the least-square residuals, r, are shown in panel (b), while panel (c) shows the histogram of the residual distribution.

Figure 2 shows that the range of amplitudes detected by SAMMER covers a dynamic range of masses for which s is not constant, violating one of the hypotheses on which Equation (2) is based. Indeed, the deviation from the straight line is attributed to two major factors: (i) for small amplitudes, the cumulative distribution gently tends to a constant value as the amplitudes approach the minimum value that the radar is capable to measure ($\sim 10^3$ for SAMMER); and (ii) as the amplitude increases, the echoes regime migrates from predominantly underdense to predominantly overdense, causing a progressive change of the slope from $1 - s$ to $4(1 - s)$. Blaauw et al. (2011b) noted that the region of transition from under- to overdense echoes expands (which is equivalent to saying that the linear part of the curve shortens) when echoes detected at different ranges are mixed. The separation between these different regimes is not sharp which affects the linear nature of the portion of the distribution attributed to underdense echoes biasing the determination of s. In order to overcome this, Blaauw et al. (2011b) as well as Pokorný & Brown (2016) restricted their study to events that were detected within a narrow range which was chosen somewhat arbitrarily. Similarly to those authors, we have restricted our analysis to ranges between 100 and 130 km.

As pointed out by Pokorný & Brown (2016), the simple problem of fitting a straight line through a set of points is challenged by the more complex problem of determining the minimum and maximum limits of the amplitude range within which Equation (2) is valid. That is, what part of the measured cumulative distribution is due to only the detection of underdense echoes. This problem is usually addressed through the statistical analysis of the residual distribution. Basically, the range of amplitudes is reduced until the residual distribution approaches the normal distribution as close as possible. Typically, the χ-square test is applied to judge the normality of the residual distribution. The application of this method requires the search for a balance between narrowing the range of amplitudes that is necessary to achieve normally distributed residuals, and maintaining a sample large enough so that the number of points contained within it has statistical significance. A good example of this can be found in Pokorný & Brown

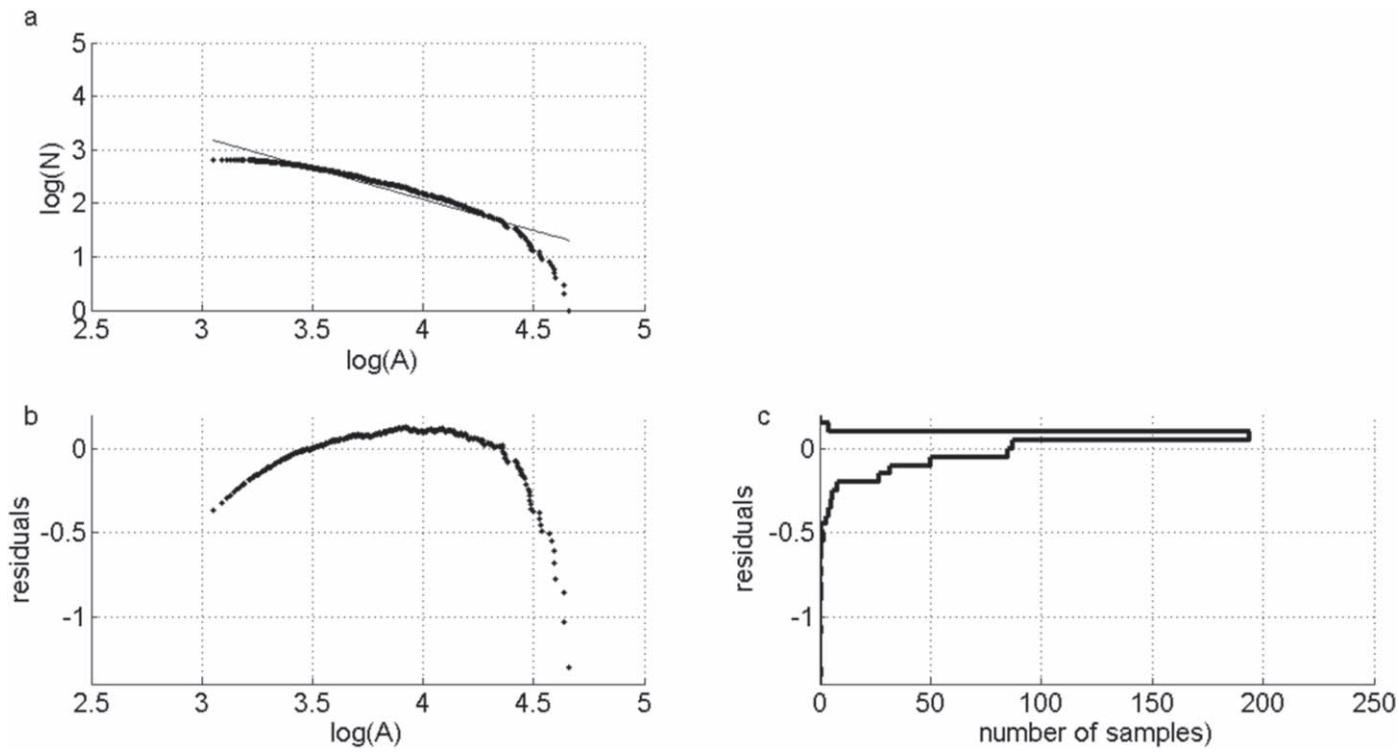

Figure 2. (a) Plot of log N vs. log A for echoes recorded by SAMMER with solar longitudes between 50° and 51° in 2008, (b) residuals after fitting a straight line, and (c) residuals' distribution.

(2016), who utilized the MultiNest Bayesian interference tool (Feroz et al. 2013) to perform this task.

The following paragraphs describe the methodology that we have applied in this work. Given $x_i = \log A_i$ and $y_i = \log N_i$, where $N_i = \sum_{j=1}^{M} n_j$ and n_j is the number of echoes in the range $(x_i - \Delta x/2, x_i + \Delta x/2)$, we adopt $\Delta x = 0.001$, which provides approximately 1800 samples per degree of λ_0. In addition and in order to increase the statistical significance of the sample, we process the data packages of 10° of solar longitude, which leads to the following set of condition equations:

$$\left.\begin{array}{l} y_{1,1} = p.x_{1,1} \ +\alpha_1 \cdots +0 \\ \quad\vdots \qquad\quad \vdots \qquad \ddots \\ y_{1,n1} = p.x_{1,n1} +\alpha_1 \cdots +0 \end{array}\right\} \lambda_0 = 1^\circ$$
$$\vdots \qquad\quad \vdots \qquad \ddots$$
$$\left.\begin{array}{l} y_{10,1} = p.x_{10,1} +0 \cdots +\alpha_{10} \\ \quad\vdots \qquad\quad \vdots \qquad \ddots \\ y_{1,n1} = p.x_{1,n1} +0 \cdots +\alpha_{10} \end{array}\right\} \lambda_0 = 10^\circ,$$

where the first subscript identifies λ_0 and the second identifies the sample within each daily data block. In this way, 11 parameters (namely p and $\alpha_1 \cdots \alpha_{10}$) are simultaneously estimated by least-squares methods out of approximately 18,000 samples contained in 10 degrees of λ_0. It is important to note that this method leads to the estimation of a different proportionality constant for each day, but at a single value of the mass index for the 10 days. Similarly than Figure 2, Figure 3 shows the results of the fitting routine obtained by applying this method with data with solar longitudes between 50° and 60° in 2008.

It is evident from this figure, without the need for additional statistical testing, that the residuals shown in Figure 3 are not normally distributed. It is remarkable, for example, the asymmetry of the distribution, which shows negative residues much more dispersed than positive. This could be quantified, for example, by computing the Fisher–Pearson coefficient of skewness, which for this distribution reaches a value as large as −2.9. Our first step for the residual distribution to approach normality is to improve its symmetry with respect to zero. For this purpose, we calculate the mean, μ_+, and the standard deviation, σ_+, of the non-negative residuals and eliminate from the sample all the data whose residuals fulfill the condition $r < -\mu_+ - 3.\sigma_+$ (dashed line in the panel (c) of Figure 3). After this, we repeat the least-squares adjustment of the cleaned data set. We repeat this iteration until one of the following conditions are satisfied.

1. The χ-square test leads not to rejecting the hypothesis that the residuals are normally distributed with a level of significance of 90%; in this case, the value of the mass index arising from the last iteration is adopted as the average value representative of the 10° of solar longitude involved in the process.
2. The previous condition is not reached before the number of data in the cleaned sample reduces to less than half of the initial amount; in this case, the data sample is discarded and it is assumed that a reliable mass index for these 10° of solar longitude could not be determined.

The threshold for negative residues (i.e., $r < -\mu_+ - 3.\sigma_+$) was established empirically, following the criterion that no iteration should eliminate more than 10% of the data in the sample. Although this empirical criterion can be refined, the numerous experiments that we have performed showed no significant change in the final results if the threshold is changed. Figure 4 shows analogous results as the preceding figure after reaching the convergence of the iterative process

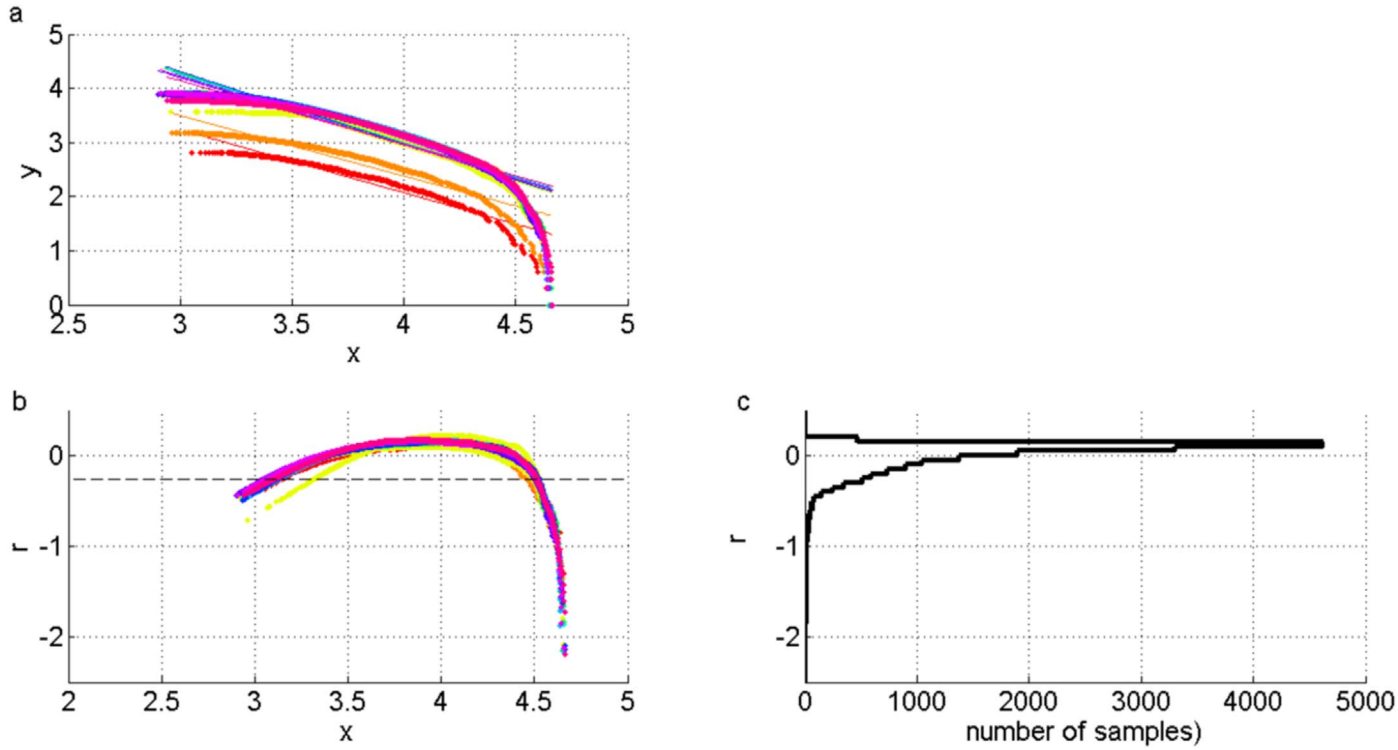

Figure 3. (a) Plot of $y = \log N$ vs. $x = \log A$ for echoes recorded by SAMMER with solar longitudes between 50° and 60° in 2008, (b) residuals after fitting straight lines according to Equation (3), and (c) residuals' distribution.

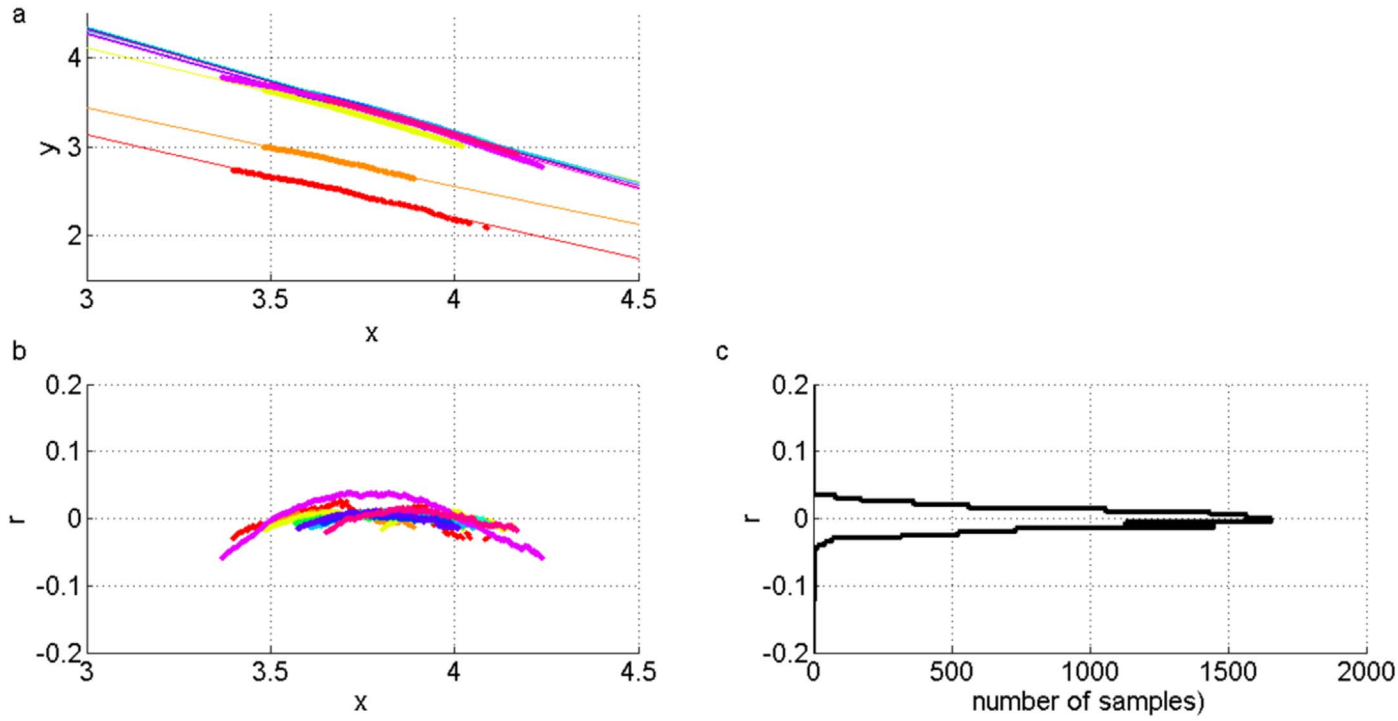

Figure 4. (a) Results for the cleaned sample of data recorded by SAMMER with solar longitudes between 50° and 60° in 2008: (a) plot of $y = \log N$ vs. $x = \log A$, (b) residuals after fitting straight lines, and (c) residuals distribution.

just described. For these 10° of solar longitude (arbitrarily chosen to show an example of the application of our method) the mass index resulted as $s = 2.0$.

4. Results

We apply the method described in the previous section to ~11 yr of SAAMER observations covering the period 2008 April 13 to 2018 December 31. Since in this work we focus only on determining the differential mass index, s, of the

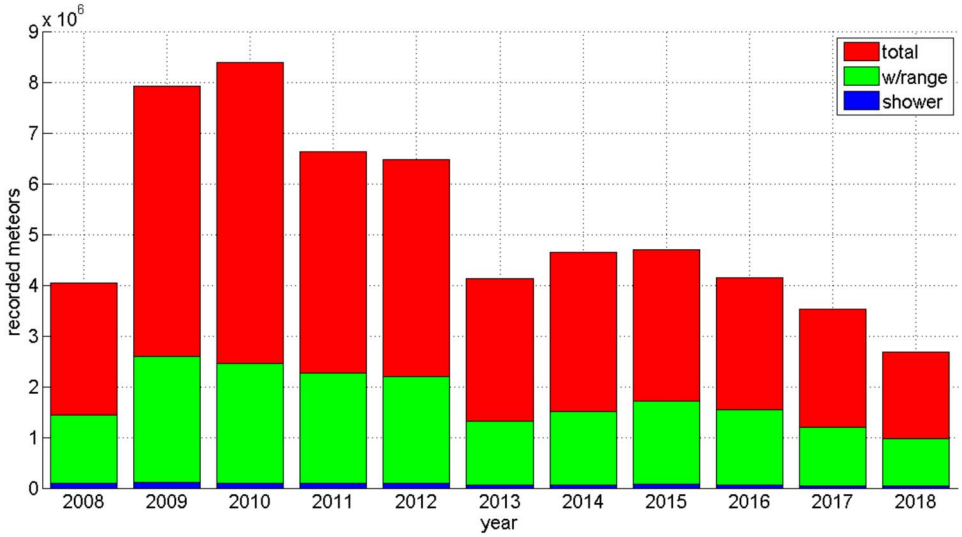

Figure 5. Number of meteors recorded by SAAMER during the 11 yr utilized in this study.

sporadic environment in the southern hemisphere, we exclude from the data those meteors which are potentially originating from strong showers. For this purpose we adopt the list of more than 60 showers detected by SAAMER using its orbital determination capabilities reported by Pokorný et al. (2017). This list comprised of approximately 30 previously known and 30 new showers (See Tables 2 and 3 of Pokorný et al. 2017), which were identified using a wavelet searching methodology on an orbital data set of approximately a total of a million orbits. This methodology has been used by several authors to perform equivalent searches (Galligan & Baggaley 2002; Brown et al. 2008; Pokorný et al. 2017; Schult et al. 2018). One of the parameters this methodology provides is the weighting factor, w_c, used as a proxy of the strength of the shower. For this work we selected 31 showers which have a $w_c \geqslant 100$. Since the data we use in this study lacks directional information (single station observations), we consider a meteor to be potentially originating from one of these 31 showers if the R.A. and decl. (δ) of the meteor echo determined from its elevation and azimuth is 90° (±5°) from the center of the shower radiant and within the solar longitudes during which the shower is active (also Tables 2 and 3 of Pokorný et al. 2017). This is because underdense echoes are detected perpendicular to their direction of motion and thus the meteor radiant, echo point, and the radar should form a 90° angle (Janches et al. 2013).

Figure 5 presents statistics of the amount of meteors detected by SAAMER: the red bars are the meteors recorded every year, green bars are the meteors with ranges between 100 and 130 km (which were the ones used in this work), and blue bars are the meteors attributed to 1 of the 30 selected showers. SAAMER recorded more than 57 million meteors during the 11 yr included in this study; out of these, almost 20 million were detected at ranges between 100 and 130 km. Just under a million of those meteors were identified as potentially belonging to a meteor shower. Approximately 12% of the meteors in the range of 100–130 km satisfy the appropriate conditions to perform this study.

Figure 6 shows the estimated differential mass indexes as a function of the continuous solar longitude (i.e., the solar longitude counted continuously from 2008). It can immediately be observed in this figure the increasing trend present in our results as a function of time. A simple linear adjustment of the data points in Figure 6 yields to a mean value of 2.20 and an increasing linear trend of 0.011 yr^{-1}. This mean value is in agreement with the values reported in the northern hemisphere using CMOR observations by Blaauw et al. (2011b), but somewhat larger than the revised values reported by Pokorný & Brown (2016) and the estimates in the southern hemisphere reported by Baggaley (1999) and Galligan & Baggaley (2004) utilizing only half of a million detections from the AMOR system.

Interannual fluctuations in the mass index determined using the peak amplitude cumulative distribution as a proxy of the meteor electron density and mass have also been reported by Pokorný & Brown (2016), who suggested they are likely caused by solar activity affecting the mass density of the atmosphere at meteor ablation heights. It is worth noting that those authors reported data collected over 5 yr, as compared to our study, where we explore data comprise of an entire solar cycle (11 yr), including the years investigated by Pokorný & Brown (2016). Figure 7 displays the peak of the daily altitude distribution of the selected meteor sample used in this study. It can be seen that although there is both an interannual and seasonal variability of the peak altitude, it is only of the order of ∼2 km. Considering that the selected echoes are within a 20 km interval in range and altitude, such variability should not affect the results considerably. Nevertheless, if the trend shown in Figure 7 would be due to solar variability, it should show a cyclic behavior rather than a constant increase, since the observations were performed during an entire solar cycle. Another effect that is known to bias the results and increase the mass index is the so-called initial trail radius effect (Jones & Campbell-Brown 2005) that attenuates the radar signal when the size of the trail is comparable to the radar wavelength. Pokorný & Brown (2016) however used a comparison of radar and optical mass and altitude distributions measured with CMOR and CAMO showing that CMOR mass-index distributions are minimally affected by the initial trail radius. Given the similarity of SAAMER and CMOR (both SKiYMET systems) and relative similar transmitting frequencies (29.85 and 38.15 MHz for CMOR and 33.55 MHz for SAAMER), we also assume in this work that the trail radius effect will not significantly affect our results.

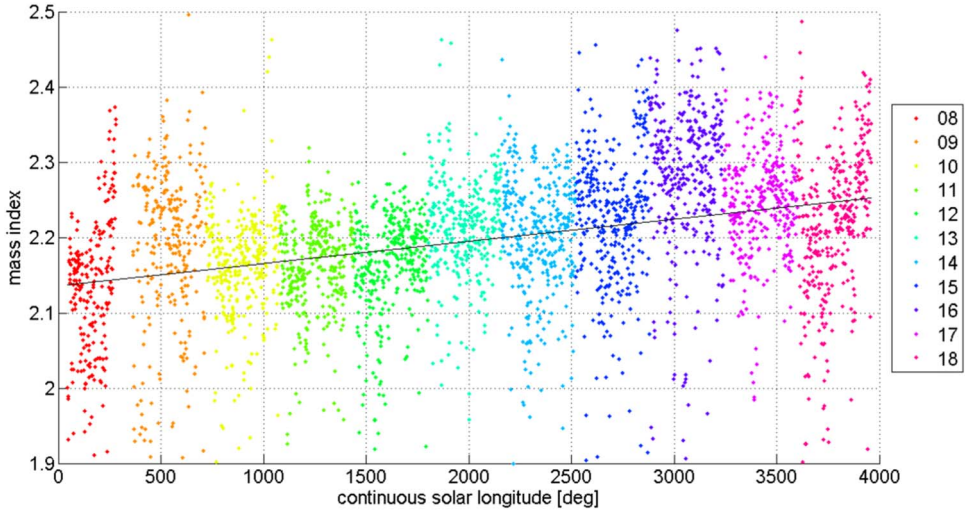

Figure 6. Estimated mass indexes as a function of the continuous solar longitude.

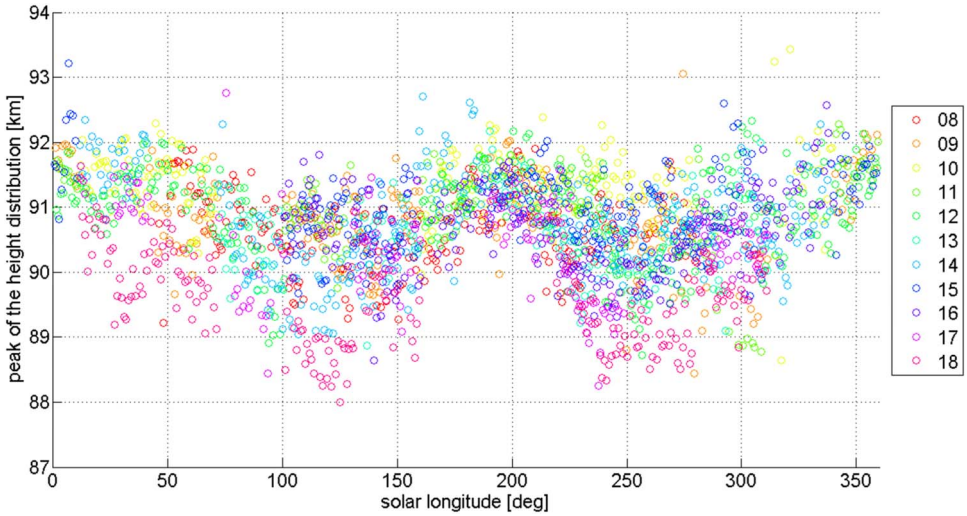

Figure 7. Height of the peak of the altitude distribution as a function of the solar longitude.

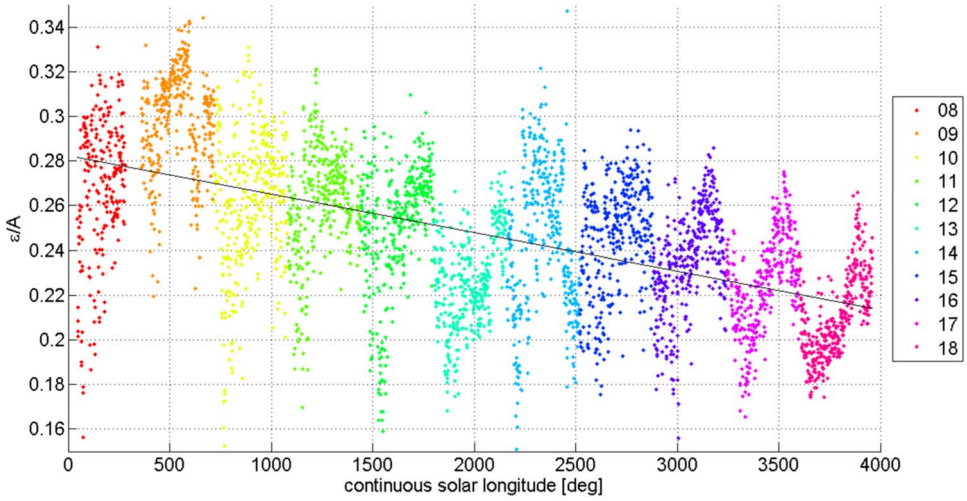

Figure 8. Daily mean value of the inverse S/N as a function of the continuous solar longitude.

A parameter that has not been, at least explicitly, discussed in the works by AMOR and CMOR is the role that the system noise can have in biasing the determination of s using the echoes amplitudes as a proxy of the electronic density and mass. As mentioned earlier, the radar processing software records for every meteor not only the maximum amplitude,

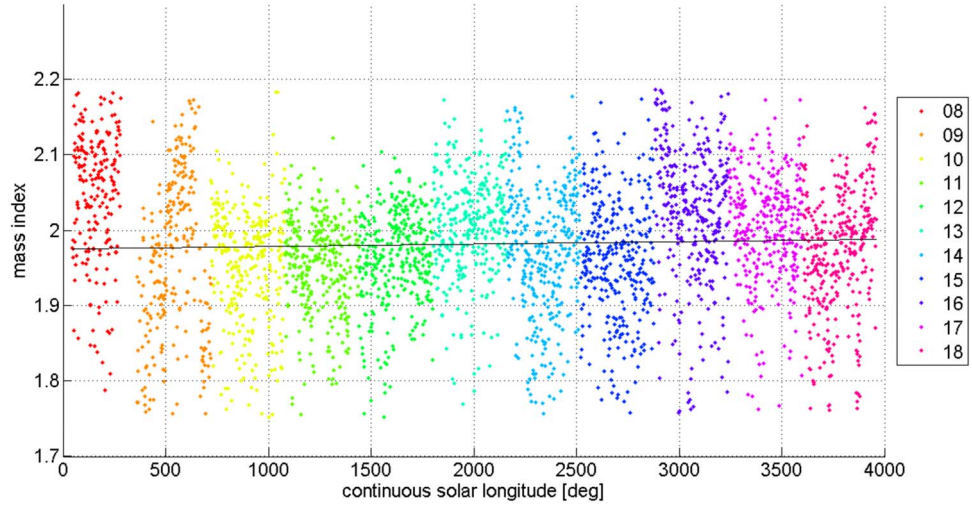

Figure 9. Estimated mass indexes after removing the noise from the recorded amplitudes, as a function of the continuous solar longitude.

which is an average of the maximum amplitude recorded at each of the five receiving antennas, but also the mean S/N represented in this work as A/ϵ, where A is the peak amplitude of the meteor echo and ϵ is the noise. Figure 8 shows the daily mean value of the inverse of S/N represented as a function of the continuous solar longitude. In can be seen in this figure the presence of a seasonal variability which would be attributed to various natural and environmental sources. An additional decrease on the system performance revealed by the decreasing trend of the inverse of S/N of the order of $-0.006\ \mathrm{yr}^{-1}$ is also evident in this figure.

The fact that the increase in the resulting mass index seems to be directly correlated with the decrease of the inverse S/N suggests that using the cumulative distribution of the meteor echo peak amplitude as a proxy of the incoming mass distribution is affected by the system noise, and thus without properly addressing this effect the results of the mass index can be biased to higher values. It is unclear how previous work have corrected (or not) for this effect as it is never explicitly addressed. Here, we proceed to correct the amplitudes measured by SAMMER by removing the noise recorded by the instrument, and determining the corrected cumulative distribution using Equation (2) from the cumulative distribution of the corrected amplitude A^* calculated as $A^* = A.(1 - \epsilon/A)$. We then use the corrected values of $x^* = \log A^*$ and $y^* = \log N^*$ in Equation (3). The resulting corrected differential mass indexes as a function of the continuous solar longitude are shown in Figure 9. The increasing trend noted in Figure 6 has essentially disappeared. A simple linear adjustment performed on these new mass index estimates yield to an average value of 1.98 (slightly lower than the previous one but now in agreement with those reported by Pokorný & Brown (2016)) and linear trend of $0.001\ \mathrm{yr}^{-1}$, which is essentially negligible.

5. Discussion

Figure 10 shows the same results of Figure 9, but superimposing the 11 yr covered by the SAAMER observations, where each year is identified by a different color. In addition, the thick black line represents the average value of the 11 yr for every solar longitude. The mean value determined from the black curve is 1.98 ± 0.03. In addition, Table 1 presents the resulting mean values of the mass index per year. We will limit the comparison of our results for the purpose of the discussion in this section to those reported by the most recent studies of the meteoroid environment differential mass index. Specifically, we will only focus on the reports by Blaauw et al. (2011b) and Pokorný & Brown (2016) using CMOR observations in the northern hemisphere and those by Baggaley (1999) and Galligan & Baggaley (2004) using observations from AMOR in the southern hemisphere. There are various reasons for this: (1) the similarity of the observation methodologies and systems employed (i.e., radars and SKiYMET for the case of CMOR and SAAMER); (2) the mass range of the particles observed; (3) the statistical sample size (from 0.5 to several millions data points); and (4) the period of observations (i.e., all studies have multi-year observations). In addition, the works in the northern hemisphere were performed during periods that overlap with SAAMER's observations. These studies have reported comparisons with previous works and the reader can refer to those for details and results of earlier works.

Blaauw et al. (2011b), using a manual method for fitting the cumulative distributions, found $s = 2.17 \pm 0.07$, about 10% higher than the noise-debiased values found in this study. That work used 4 yr worth of observations (2007–2010), two and a half of which overlapped with the SAAMER study. On the other hand, Pokorný & Brown (2016) revised the CMOR results using 5 yr worth of observations (2011–2015), a period that also overlapped with our study. The authors introduced an automated methodology to fit the cumulative distributions using Bayesian statistics and found a somewhat smaller value of $s = 2.015 \pm 0.072$, which is in full agreement with the value found in this study. Interestingly, the analysis by Blaauw et al. (2011b) was performed by a sample in which six major showers were filtered out, while the work of Pokorný & Brown (2016) did not remove showers in their final results. Thus it is possible that the lower value of the latter may be influenced by the presence of showers in their sample that would bring their mean s to lower values. If that is the case and the CMOR measurements are equally affected by the noise as we showed to be the case for SAAMER, then their values could be somewhat overestimated. For the case of the southern hemisphere, the AMOR study by Galligan & Baggaley (2004) in which only half of a million meteor echoes were utilized, resulted in $s = 2.027 \pm 0.006$, also in good agreement with

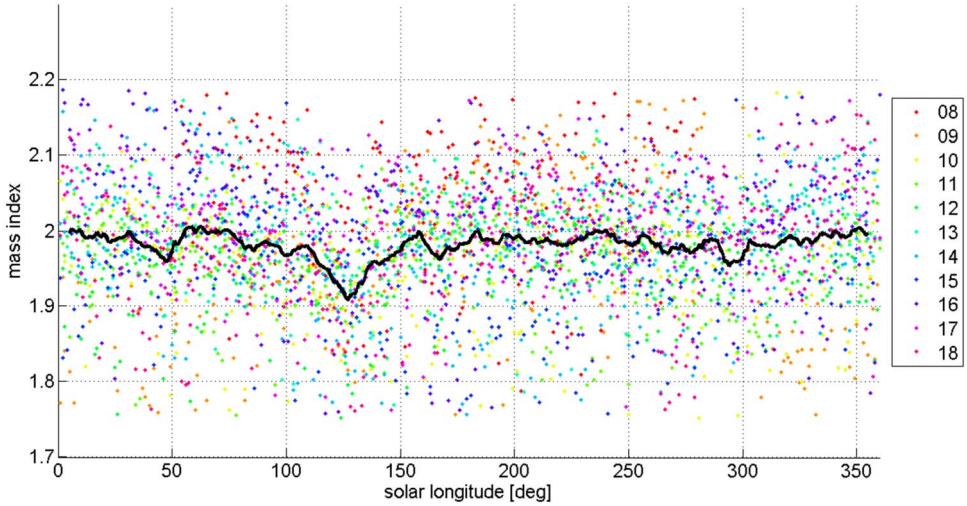

Figure 10. Estimated mass indexes after removing the noise from the recorded amplitudes, as a function of the solar longitude for the 11 yr covered by this study. The solid black line is the moving average with a window of 10° of solar longitude.

Table 1
Mean Values per Year

Year	Mass Index Mean Value
2008	2.047 ± 0.084
2009	1.964 ± 0.106
2010	1.953 ± 0.076
2011	1.955 ± 0.061
2012	1.962 ± 0.062
2013	2.005 ± 0.066
2014	1.971 ± 0.086
2015	1.961 ± 0.079
2016	2.020 ± 0.090
2017	2.002 ± 0.071
2018	1.974 ± 0.082

our result. It is interesting to note that AMOR transmitted 100 kW on a very narrow radiation pattern of 2° (Baggaley et al. 1994), which made it sensible to very small meteors (limiting radio magnitude of +14, limiting mass of 0.3 μg); this is about 2 orders of magnitude lower than CMOR which transmits 6–12 kW distributed in an all-sky radiation pattern. SAAMER on the other hand sits in the middle of these two systems, with 5–10 times more transmitted power than CMOR and only 1.6 times less power than AMOR. On the other hand, the radiation pattern of SAAMER is not as focused as AMOR and not as widely distributed as CMOR. Thus, the mass range detected by SAAMER is most likely an overlap between CMOR and AMOR. Efforts to calibrate SAAMER to detect the meteoroid mass range are undergoing. It is important to note that all these relatively newer studies provide values significantly smaller than in the past, which have ranged from $s = 2.2$–2.5 (Hawkins & Upton 1958; Simek & McIntosh 1968). In fact, flux models such as those reported by Grün et al. (1985) use values as high as $s = 2.34$ for the submilligram mass range and Pokorný & Brown (2016) have suggested that shallower values of s should occur at larger masses than previously assumed. This study further emphasizes this to be the case.

The importance of a difference between an $s = 2.0$–2.1 can be easily quantified if the classical relation between the differential size (α) and mass (s) index is assumed as (P. Pokorný 2019, personal communication)

$$\alpha = 3s - 2. \tag{3}$$

In terms of the number of particles, a 0.1 difference in s will introduce a $10^{0.3}$ difference in the number particles for every decade of the power law. So if particles with sizes between 1000 and 10 μm are considered, then the larger s would result in about four times more particles. Such differences could be important, for example, when trying to reconcile dynamical models with meteor head-echo observations, in particular of very small particles, using high-power and large aperture radars (Janches et al. 2017).

Regarding seasonal variability, after removing the strongest showers and correcting by the system noise it is clear from Figure 10 that the SAAMER's results are constant throughout the year. It is important to note, however, that the seasonal and interannual variability are larger than the quoted errors in Table 1. This is because those errors are the results of the least-square fits and thus they do not take into account the variability. A similar argument can be made of the values reported by Pokorný & Brown (2016). There is, however, a small dip that seems to repeat every year at about $\lambda_0 \sim 125°$. This is the time when the Southern δ Aquiriids (SDA) meteor shower reaches it maximum in terms of SAAMER's detection according to Pokorný et al. (2017). Since the SDA is one of the strongest showers detected by SAAMER, it is possible that the methodology to remove meteors from showers used in this study is not sufficiently effective and thus some contamination still dominates at the time of the shower maxima, biasing the results toward lower values of s. Blaauw et al. (2011b) on the other hand found that the CMOR measurements showed a slight change on s through the year. The authors also found some small differences between the individual mass indices of the five sporadic sources that CMOR is able to detect. Specifically, they found that the average sporadic mass index shows a minimum between $\lambda_0 \sim 200°$ and 300° (mid-January) and then increasing toward $\lambda_0 \sim 0$ (mid-March) and some continue to increase or remain high after this point. Since the authors only removed six major showers, they speculate that some of this variability may be due to contamination from smaller showers that were not removed from the data, which

would agree somewhat with our findings. That is, since we removed 30 showers that include the major and some weaker ones, such variability would then not be present in our study. Pokorný & Brown (2016) on the other hand did not remove showers from their sample and associated some of the major seasonal variation of s to major showers. For the case of southern hemisphere observations, Baggaley (1999) showed also some variability with a dip also at the time of the SDA. However, that study did not remove showers and was very limited with the inclusion of data from particular local times, so further comparisons with the SAAMER study at this stage are premature. There are two points that are important to note regarding the seasonality of s. First, the variability reported by Blaauw et al. (2011b) is within the reported errors so it can be argued that such seasonality is, at least in part, an artifact of the measurements, and second, Figure 8 clearly shows that at least at SAAMER, the S/N shows also a seasonal signature. So it is very likely that, since it appears that the system noise has not been taken into account in the CMOR or AMOR studies, that some of this seasonality is due to contamination due to the clear sensitivity to system noise of the methodology of determining s using the echo amplitude as a proxy.

6. Conclusions

In this manuscript we presented determinations of the meteoroid differential mass index, s, using practically an entire solar cycle worth of meteor observations from SAAMER. The parameter is calculated from the linear portion of the cumulative distribution of radar-detected underdense meteor peak amplitudes which is used as a proxy of the meteor electron density and mass. Finding the limits of the linear portion of such distribution is challenging due to the contamination of overdense and transitional echoes as well as the system sensitivity (Blaauw et al. 2011b; Pokorný & Brown 2016). We developed an autonomous statistical technique, similar but simpler than that reported by Pokorný & Brown (2016), to determine this parameter. Unlike previous studies, we found that the system noise biased the results and overestimate s. In general we found that a value of $s = 2.0$ represents SAAMER's results in general agreement with recent studies performed in the northern and southern hemispheres (Baggaley 1999; Galligan & Baggaley 2004; Blaauw et al. 2011b; Pokorný & Brown 2016). We explore both the index interannual and seasonal variability and, unlike previous studies, we found it to be constant except during the presence of the Southern δ Aquariids meteor shower which is so strong that it dominates the meteor counts when present. Although statistical method to fit the amplitude distributions leads to small errors, our study indicates that using the maximum echo amplitude for these studies is not ideal as it can be biased by many factors which make the inaccuracies larger than the precision estimated from the fitting routine. The development of a method that results in a more direct estimate of the electron line density is required which takes into account range, gain pattern, system noise, etc. (R. Weryk 2019, personal communication).

D.J.'s work is supported by the NASA Solar System Observation (SSO) Program and the NASA Engineering and Safety Center (NESC). SAAMER's operation is supported by NASSA SSO, NESC, and NSF grant AGS-1647354. The authors appreciate the invaluable support of Carlos Ferrer, Gerardo Connon, and Luis Barbero with the operation of SAAMER. We thank R. Weryk, B. Vandepeer, and B. Fuller for useful discussions.

ORCID iDs

D. Janches https://orcid.org/0000-0001-8615-5166

References

Ade, P. A. R., Aghanim, N., Armitage-Caplan, C., et al. 2014, A&A, 571, A14
Baggaley, W., Bennett, R., Steel, D., & Taylor, A. 1994, QJRAS, 293
Baggaley, W. J. 1999, in Proc. Int. Conf. Meteroids 1998, ed. W. J. Baggaley & V. Porubcan (Stará Lesná: Ast. Inst. Slovak Academy Sci.), 311
Blaauw, R. C., Campbell-Brown, M. D., & Weryk, R. J. 2011a, MNRAS, 414, 3322
Blaauw, R. C., Campbell-Brown, M. D., & Weryk, R. J. 2011b, MNRAS, 412, 2033
Brown, P., Weryk, R. J., Wong, D. K., & Jones, J. 2008, EM&P, 102, 209
Campbell-Brown, M., & Wiegert, P. 2009, M&PS, 44, 1837
Feroz, F., Hobson, M. P., Cameron, E., & Pettitt, A. N. 2013, arXiv:1306.2144
Fritts, D. C., Janches, D., & Hocking, W. K. 2010a, JGRD, 115, 19123
Fritts, D. C., Janches, D., Iimura, H., et al. 2010b, JGRD, 115, 18112
Fulle, M., Colangeli, L., Mennella, V., Rotundi, A., & Bussoletti, E. 1995, A&A, 304, 622
Fulle, M., Marzari, F., Della Corte, V., et al. 2016, ApJ, 821, 19
Galligan, D. P., & Baggaley, W. J. 2002, in IAU Coll. 181, Dust in the Solar System and Other Planetary Systems, ed. S. F. Green (Oxford: Pergamon), 48
Galligan, D. P., & Baggaley, W. J. 2004, MNRAS, 353, 422
Grün, E., Zook, H., Fechtig, H., & Giese, R. H. 1985, Icar, 62, 244
Hawkins, G. S. 1956, AJ, 61, 386
Hawkins, G. S., & Upton, E. K. L. 1958, ApJ, 128, 727
Hocking, W. K., Fuller, B., & Vandepeer, B. 2001, JASTP, 63, 155
Hocking, W. K., Thayaparan, T., & Jones, J. 1997, GeoRL, 24, 2977
Janches, D., Close, S., Hormaechea, J. L., et al. 2015a, ApJ, 809, 36
Janches, D., Hocking, W., Pifko, S., et al. 2014, JGRA, 119, 2269
Janches, D., Hormaechea, J. L., Brunini, C., Hocking, W., & Fritts, D. C. 2013, Icar, 223, 677
Janches, D., Pokorný, P., Sarantos, M., et al. 2018, GeoRL, 45, 1713
Janches, D., Swarnalingam, N., Carrillo-Sanchez, J., et al. 2017, ApJ, 843, 1
Janches, D., Swarnalingam, N., Plane, J. M. C., et al. 2015b, ApJ, 807, 13
Jones, J. 1968, CaJPh, 46, 1101
Jones, J., & Campbell-Brown, M. 2005, MNRAS, 359, 1131
Jones, J., Webster, A. R., & Hocking, W. K. 1998, RaSc, 33, 55
Love, S., & Brownlee, D. E. 1993, Sci, 262, 550
McIntosh, B. A., & Simek, M. 1969, CaJPh, 47, 7
McKinley, D. W. R. 1961, Meteor Science and Engineering (New York: McGraw-Hill)
Nesvorný, D., Janches, D., Vokrouhlický, D., et al. 2011a, ApJ, 743, 129
Nesvorný, D., Jenniskens, P., Levison, H. F., et al. 2010, ApJ, 713, 816
Nesvorný, D., Vokrouhlický, D., Pokorný, P., & Janches, D. 2011b, ApJ, 743, 37
Pokorný, P., & Brown, P. G. 2016, A&A, 592, A150
Pokorný, P., Sarantos, M., & Janches, D. 2017, ApJL, 842, L17
Pokorný, P., Sarantos, M., & Janches, D. 2018, ApJ, 863, 31
Pokorný, P., Vokrouhlický, D., Nesvorný, D., Campbell-Brown, M., & Brown, P. 2014, ApJ, 789, 25
Rotundi, A., Sierks, H., Della Corte, V., et al. 2015, Sci, 347, aaa3905
Schult, C., Brown, P., Pokorný, P., Stober, G., & Chau, J. L. 2018, Icar, 309, 177
Sekanina, Z. 1976, Icar, 27, 265
Simek, M., & McIntosh, B. A. 1968, in IAU Symp. 33, Physics and Dynamics of Meteors, ed. L. Kresak & P. M. Millman (Dordrecht: Reidel), 362
Webster, A. R., Brown, P. G., Jones, J., Ellis, K. J., & Campbell-Brown, M. 2004, ACPD, 4, 1181
Weiss, A. A., & Smith, J. W. 1960, MNRAS, 121, 5
Weryk, R. J., Campbell-Brown, M. D., Wiegert, P. A., et al. 2013, Icar, 225, 614